ACS APPLIED MATERIALS & INTERFACES

Research Article

Cite This: ACS Appl. Mater. Interfaces XXXX, XXX, XXX−XXX

www.acsami.org

Enhanced Organic Photovoltaic Performance through Modulating Vertical Composition Distribution and Promoting Crystallinity of the Photoactive Layer by Diphenyl Sulfide Additives

Jianfeng Li,*[,†,‡] Yufei Wang,[†,‡] Zezhou Liang,[†,‡,§] Ningning Wang,[‡] Junfeng Tong,[†] Chunming Yang,[∥] Xichang Bao,*[,†,§] and Yangjun Xia*[,†]

[†]School of Materials Science and Engineering, Lanzhou Jiaotong University, Lanzhou 730070, P. R. China

[‡]Key Laboratory of Optoelectronic Technology and Intelligent Control of Education Ministry, Lanzhou Jiaotong University, Lanzhou 730070, China

[§]Qingdao Institute of Bioenergy and Bioprocess Technology, Chinese Academy of Sciences, Qingdao 266101, China

[∥]Shanghai Synchrotron Radiation Facility, Shanghai Institute of Applied Physics, Chinese Academy of Sciences, Shanghai 201204, China

Supporting Information

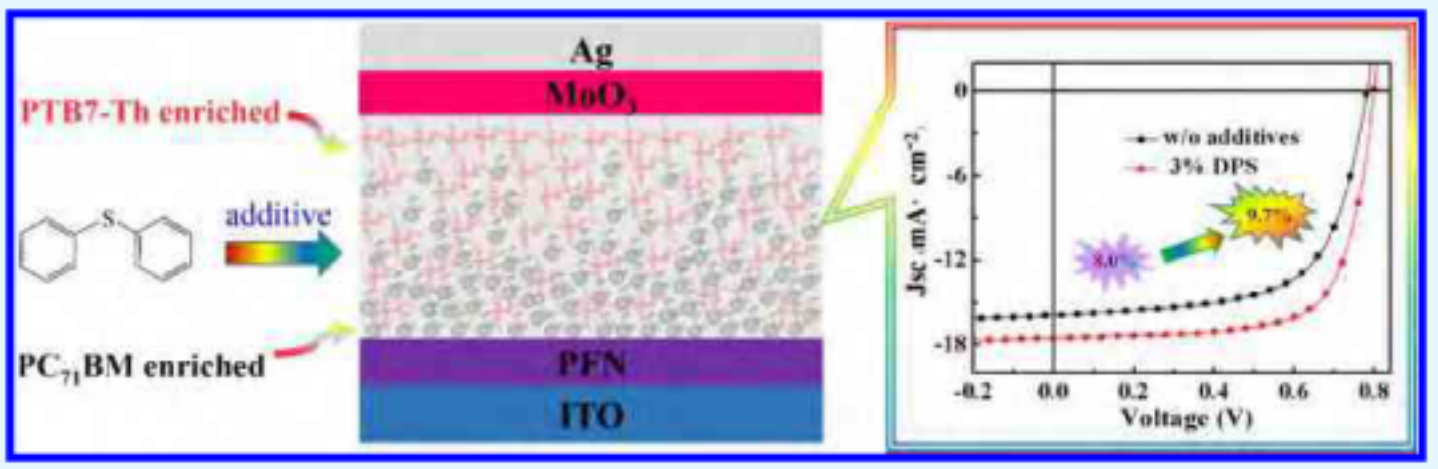

ABSTRACT: To understand the vertical phase separation in the bulk junction active layer of organic photovoltaic devices is essential for controlling the charge transfer behavior and achieving effective charge collection. Here, diphenyl sulfide (DPS) was introduced as a novel additive into the PTB7-Th:$PC_{71}BM$-based inverted polymer solar cells (PSCs), and the effect of additives on active blend films and photovoltaic characteristics was carefully studied. The results show that DPS could not only modulate the vertical composition distribution but also promote the ordered molecular packing of the photoactive layer, thus effectively improving exciton dissociation, charge transport, and collection, and thus exhibit an excellent power conversion efficiency of 9.7% with an improved fill factor (>70%) after using 3% DPS additive. The results show that the DPS solvent additive can effectively adjust the vertical phase distribution and crystallinity of blend films and improve the photovoltaic performance of the inverted organic photovoltaic devices.

KEYWORDS: *organic photovoltaic devices, additive, diphenyl sulfide, vertical composition distribution, crystallinity*

1. INTRODUCTION

Organic photovoltaic devices were considered prospective candidates for renewable energy technology owing to their light weight, compatible with flexible substrates, semitransparency, and large area fabrication. To boost up power conversion efficiency (PCE), it was necessary to fine tune the photoactive layer's morphology in photovoltaic devices.[1−6] The ideal morphology of the photoactive layer should have the feature of a good bicontinuous interpenetrating network and suitable phase-separated domains with high purity. This provides not only sufficient interfaces for efficient exciton separation but also long enough channels for efficient charge carrier transport to the corresponding electrodes, and thus reducing free charge recombination.[7−13] In addition, the appropriate surface composition of the photoactive layer in polymer solar cells (PSCs) also contributes to effective charge collection. Therefore, the photoactive layer should enrich the donor at the anode side[14] and enrich the acceptor at the cathode side.[15,16] However, bulk morphologies and composition distribution of the photoactive layer were strongly influenced by preparation conditions of thin films, such as the properties of the donor or acceptor material, host solvent, substrate property, post-thermal annealing, solvent annealing,[17,18] and solvent additives. Therefore, development of appropriate methods to improve the morphology and composition distribution for blend films is of great significance to improve PSCs. In particular, solvent additive is one effective and simple approach to improve the morphology and composition

Received: November 21, 2018
Accepted: January 28, 2019
Published: January 28, 2019

DOI: 10.1021/acsami.8b20466
ACS Appl. Mater. Interfaces XXXX, XXX, XXX−XXX

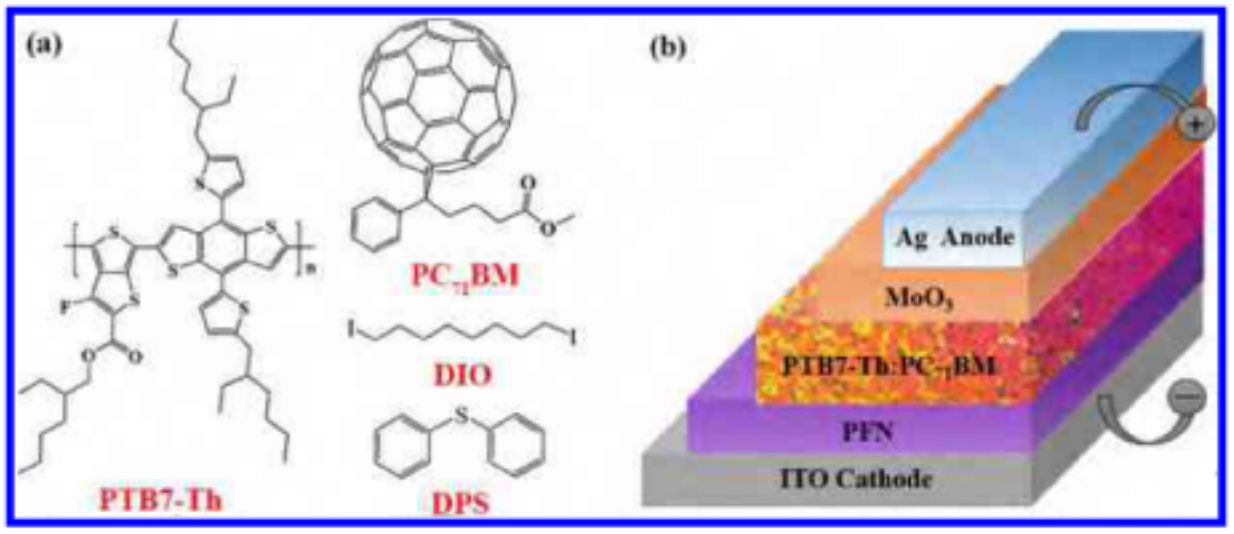

Figure 1. (a) Chemical structure of PTB7-Th, $PC_{71}BM$, DIO, and DPS and (b) the schematic diagram of PSCs.

distribution of active layers. For these reasons, substantial additives, such as 1,8-diiodooctane,[19] *N*-methyl pyrrolidone,[20] diphenyl ether,[21] 1,8-octanedithiol,[22] and chloronaphthalene,[23] were been widely used in PSCs and achieved fruitful results. When additives were added to the host solvent, the kinetics of film formation would be significantly changed, resulting in completely different morphologies.[24−26] The solubility of additives to each component of the active layer has decisive effects on phase distribution and crystallization of polymers.[27] Thus, finding new additives to control the bulk morphologies and modulate composition distribution of the donor and acceptor in the blend film is timely and highly desired.

PTBT-Th is a classical polymer in the field of PSCs and has obvious response to solvent additives. It is an ideal model system for studying the morphology, phase separation, and photovoltaic properties of polymer films. In this work, a new type of high-boiling point additive, diphenyl sulfide (DPS), was introduced to modulate composition distribution and to promote crystallinity of the PTB7-Th:$PC_{71}BM$ blend film. To study the mechanism of the additives on device performance, the morphology of the active layer and its vertical distribution were characterized by atomic force microscopy (AFM), transmission electron microscopy (TEM), grazing incidence wide-angle X-ray scattering (GIWAXS), water contact angle (WCA), and time-of-flight secondary ion mass spectroscopy (TOF-SIMS). Meanwhile, various electrical measurements with impedance spectroscopy (IS), the space charge limited current (SCLC), and time-resolved transient photoluminescence (TRTPL) spectra have been tested. After optimization of the DPS content, the PCE was increased from 8.0 to 9.7%, which was higher than that with 3% DIO (8.8%). The enhanced performance was ascribed to the promoted crystallinity and formed vertical phase segregation owing to the more PTB7-Th distribution on the surface of the active layer with adding 3% DPS.

2. RESULTS AND DISCUSSION

2.1. Photovoltaic Characteristics. The inverted device with indium tin oxide (ITO)/PFN/PTB7-Th:$PC_{71}BM$/MoO_3/Ag was prepared. The chemical structure of active materials and additives is displayed in Figure 1. The ITO glass substrates, PFN, MoO_3, and Ag were prepared according to our previous work.[28] The photoactive layer PTB7-Th:$PC_{71}BM$ (total concentration is 31.25 mg mL^{-1}, 1:1.5) solution was dissolved in CB. 3 vol % DIO and various concentrations of DPS (0.5−5 vol %) were added in CB, respectively.

To explore how the DPS works on the PSCs, inverted devices were fabricated with varying volume ratios of DPS from 0.5 to 5% contrast to CB. For comparison, the device with 3% DIO was also prepared. Figures 2 and S1 show the

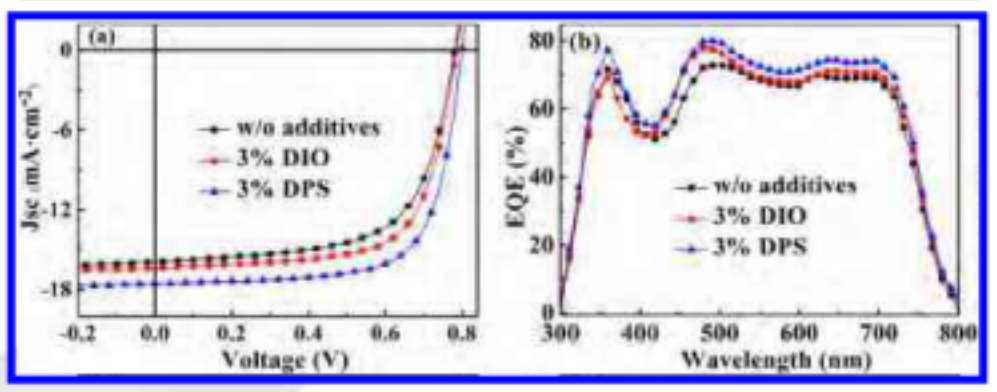

Figure 2. *J*−*V* characteristics (a) and EQE spectra of PSCs under different conditions (b).

current density−voltage (*J*−*V*) and external quantum efficiency (EQE) characteristics of PSCs under different conditions, and corresponding data are listed in Tables 1 and S1.

A poor performance with a PCE of 8.0% of the device without additive was obtained under the combined effect of these parameters of a V_{OC} of 0.78 V, a J_{SC} of 15.9 mA·cm^{-2}, and a low fill factor (FF) of 64.3%. The added 3% DIO devices relate to the controlled devices, the J_{SC} and FF of PSCs are raised from 15.9 mA·cm^{-2} and 64.3% to 16.8 mA·cm^{-2} and 68.1%, respectively, which lead to an enhanced PCE from 8.0 to 8.8%. When 3% DPS was added, J_{SC} and FF are boosted up to 17.5 mA·cm^{-2} and 70.4%, and thus a best PCE of 9.7% is obtained. In addition, the larger R_{SH} (increases from 1094.4 to 1352.4 Ω·cm^2 with 3% DPS treatment) and the smaller R_S of 4.0 Ω·cm^2 after adding 3% DPS into the CB solvent could lower the rate of charge recombination, improve charge extraction than that without additives, and decrease the probability of charge accumulation corresponding to enhancement in both J_{SC} and FF. Furthermore, the enhanced photovoltaic characteristics could be ascribed to the optimized morphology of the photoactive layer, and this will be discussed below. The EQE of the device with 3% DIO (from 400 to 700 nm) shows slight improvement owing to the morphological optimization of blend films. Furthermore, 79.94% of EQE is obtained in the device doped with 3% DPS, exhibiting much strong ability to collect carriers.

2.2. Morphological Study. To better understand the role of the additives, the surface and bulk morphology of PTB7-Th:$PC_{71}BM$ blend films prepared under different conditions were studied using AFM and TEM. It can be seen from Figure 3a−c that a lot of high-density and large aggregates of $PC_{71}BM$ were formed in the film without additives. Their size depended on the solubility of fullerene in solvents.[27−29] Because the DIO

DOI: 10.1021/acsami.8b20466
ACS Appl. Mater. Interfaces XXXX, XXX, XXX−XXX

Table 1. Characteristic Parameters of Cells Prepared under Different Conditions

additives	V_{OC} (V)	J_{SC} (mA·cm^{-2})	FF (%)	PCE (%)	R_S (Ω·cm^2)	R_{SH} (Ω·cm^2)
w/o	0.78 ± 0.01	15.9 ± 0.2	64.3 ± 0.3	8.0 ± 0.3	5.8 ± 0.5	1094.4 ± 0.4
DIO 3%	0.79 ± 0.01	16.4 ± 0.2	68.1 ± 0.4	8.8 ± 0.3	5.3 ± 0.3	1137.1 ± 0.5
DPS 3%	0.79 ± 0.01	17.5 ± 0.3	70.4 ± 0.4	9.7 ± 0.3	4.0 ± 0.6	1352.4 ± 0.5

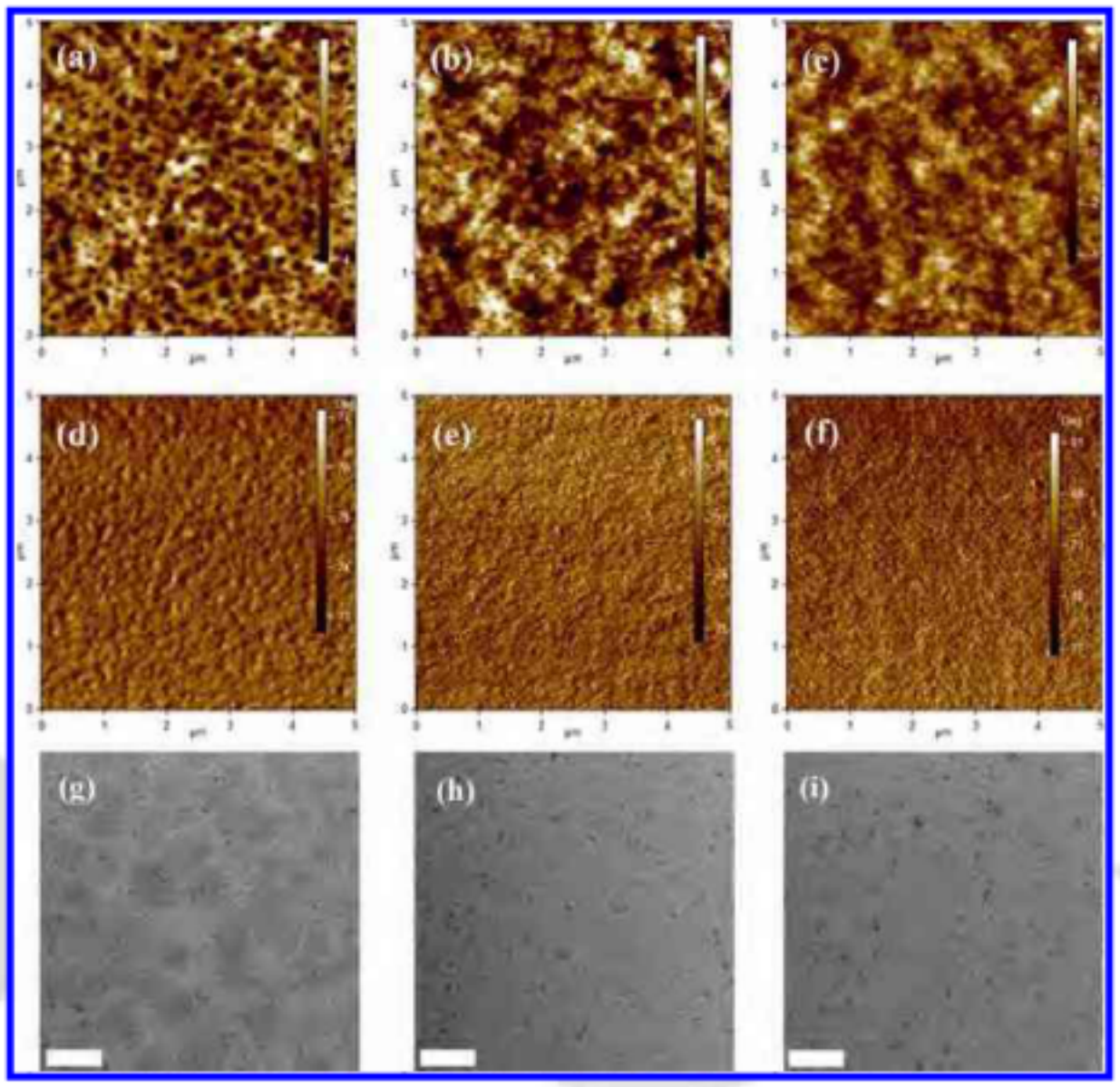

Figure 3. AFM height images (top row), AFM phase images (middle row), and TEM images (bottom row) of the blend film with different additives (the scale bar represents 200 nm), (a,d,g) without additives, (b,e,h) 3% DIO, and (c,f,i) 3% DPS.

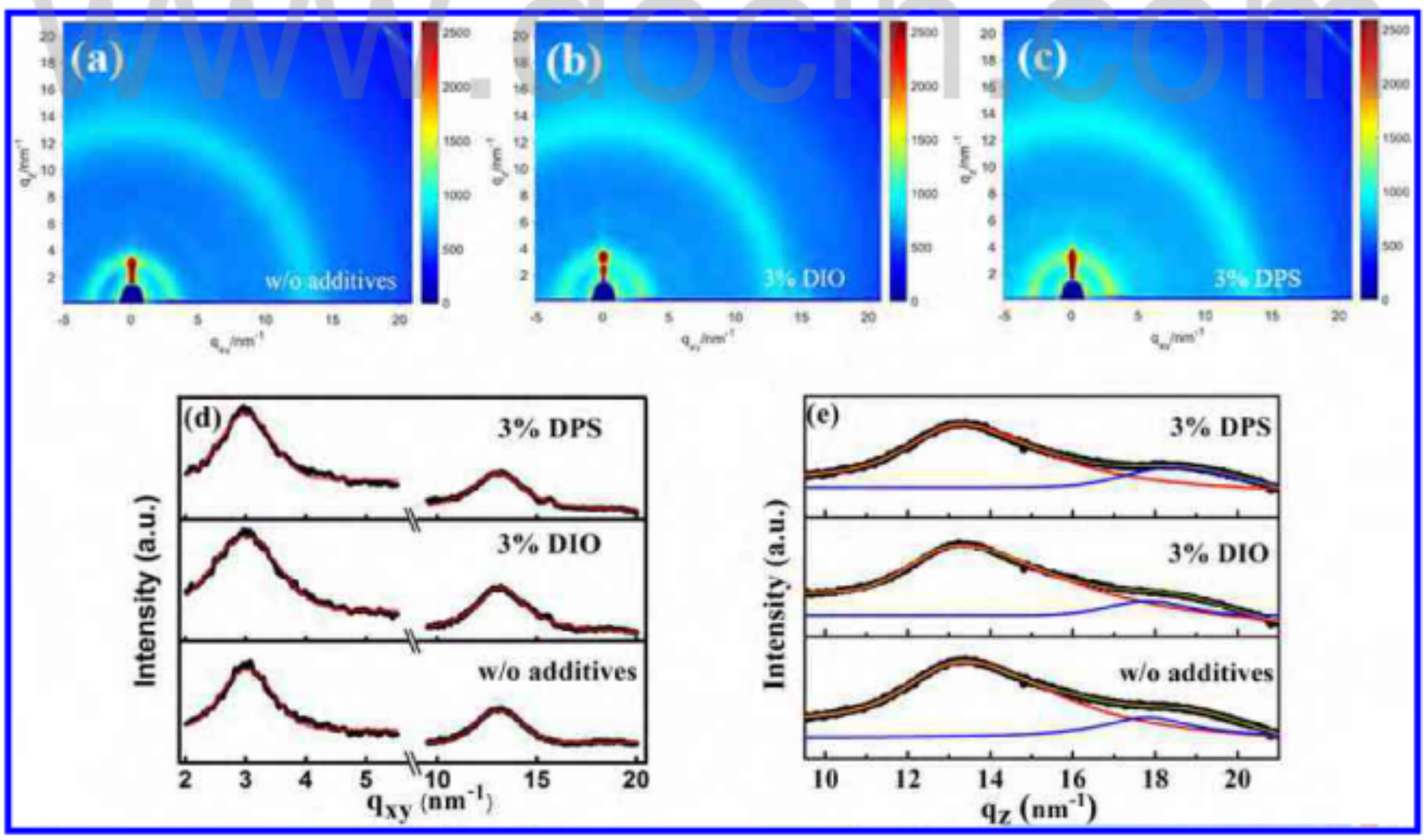

Figure 4. 2D GIWAXS patterns of blend films (a) w/o additives, (b) with DIO, (c) with DPS, (d) 1D GIWAXS profiles at the in-plane direction (d) 1D GIWAXS profiles at the out-of-plane direction.

DOI: 10.1021/acsami.8b20466
ACS Appl. Mater. Interfaces XXXX, XXX, XXX−XXX

or DPS can selectively dissolve the $PC_{71}BM$, smaller $PC_{71}BM$ domains can be formed by adding DIO or DPS into the solution. Therefore, the interface area between two components (PTB7-Th and $PC_{71}BM$) was increased because of the more uniform distribution of $PC_{71}BM$ in the PTB7-Th polymer network, thus increasing the charge separation probability.[30] Although the $PC_{71}BM$ aggregates were significantly reduced in films with solvent additives, the root-mean-square value had only small changes (1.47, 0.92, 0.95, 1.10, 1.22, 1.32, and 1.34 nm, respectively, for the DPS additive from 0 to 5%), and the surface morphology was not improved obviously.

TEM could obtain vertical phase separation information by detecting electrons running through the whole film.[31] Hence, TEM images of blend films prepared under different conditions were also obtained. As depicted in Figure 3g–i, the bright areas correspond to the polymer enrichment region and dark areas correspond to the $PC_{71}BM$ enrichment region. In the PTB7-Th:$PC_{71}BM$ thin film without additive, $PC_{71}BM$-rich domains showed strong aggregation, corresponding to low J_{SC} and poor PCE. However, after adding DIO or DPS, the obvious $PC_{71}BM$ aggregation disappeared because DIO or DPS improves the miscibility of PTB7-Th with $PC_{71}BM$.[32] Therefore, the observation in TEM could account for the corresponding enhancements in J_{SC} and FF of the device.

To further investigate the influence of additives on stacking and aggregation characteristics of PTB7-Th:$PC_{71}BM$ films, GIWAXS was conducted and illustrated in Figure 4, and all peaks were fitted with Gaussian functions to further extract the peak position and lattice constants. For the in-plane scans, there were two distinct peaks at q = 0.30 $Å^{-1}$ (d = 20.94 Å) and 1.32 $Å^{-1}$ (d = 4.76 Å), which were caused by the (100) Bragg diffraction because of lamellar packing of PTB7-Th and $PC_{71}BM$, respectively. Also, there were no tremendous differences on the pattern properties for all blended films. In the q_z scans, there were two peaks at 1.33 and 1.79 $Å^{-1}$ of blend films without additives or with DIO, which were the $\pi-\pi$ stacking peak for $PC_{71}BM$ and PTB7-Th, respectively. Meanwhile, it was interesting to observe that the q_z peak of PTB7-Th shifted to q_z = 1.85 $Å^{-1}$ of the film with DPS from q_z=1.79 $Å^{-1}$ of the film without additive or DIO, suggesting a reduction in the $\pi-\pi$ stacking distance from 3.51 to 3.40 Å, which showed that the PTB7-Th films with 3% DPS formed more compact $\pi-\pi$ stacking, consistent with the observed highest hole mobility (discussed below). Taken together, the GIWAXS results indicated that the DPS additive enhanced the lamellar and $\pi-\pi$ peak strength, indicating that the crystallinity of the films was improved.

2.3. Vertical Composition Distribution. The vertical component distribution in the photoactive layer of PSCs has important influence on phase separation and photovoltaic performance. WCA could be used to semiquantitatively calculate the content of each component of the photoactive layer surface, and the influence for different additives on the distribution of components in the photoactive layer was further understood.[33] Typical WCA (θ) measurements for neat PTB7-Th, $PC_{71}BM$, and PTB7-Th:$PC_{71}BM$ blend films with different additives were represented (Figure 5a–e). The coverage fractions (f) of PTB7-Th in the blend film surface could be calculated by the Cassie–Baxter equation[34]

$$\cos\theta = f\cos\theta_{\text{PTB7-Th}} + (1-f)\cos\theta_{PC_{71}BM}$$

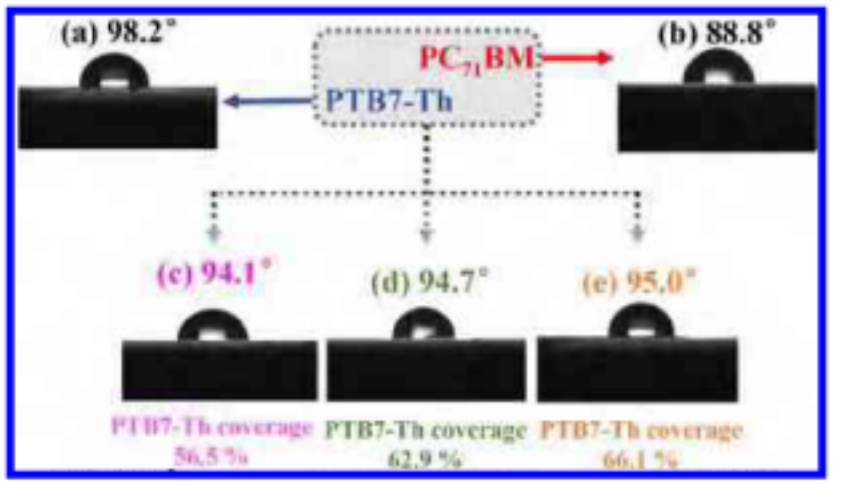

Figure 5. WCA images of the neat films: (a) PTB7-Th, (b) $PC_{71}BM$, and (c,e) blend films prepared under different conditions.

where θ, $\theta_{\text{PTB7-Th}}$, and $\theta_{PC_{71}BM}$ are the WCAs on the PTB7-Th:$PC_{71}BM$ blend films, PTB7-Th, and $PC_{71}BM$, respectively. The f was increased from 56.5% (without additives) to 62.9% (3% DIO) and finally to 66.1% (3% DPS), suggesting that more PTB7-Th might be elevated toward the upper surface of photoactive layers with 3% DPS, which should be beneficial to the transport and collection of photogenerated holes (Table 2).

In addition, PTB7-Th has the characteristic F or S element in the photoactive layer, and it is possible to analyze the variation of the yield of F^- or S^- in the whole photoactive layer with the prolonging of the sputtering time to study the vertical distribution of each component. Hence, the concentration distribution of PBT7-Th in the blend film could be directly reflected by the intensity change of the F^-or S^- signal. The depth profiles of elements F and S in the photoactive layers under different conditions were investigated by TOF-SIMS. As shown in Figures 6 and S3, the F^- or S^- signals of the blend film with 3% DIO were much stronger than those without additives and weaker than those with 3% DPS before the sputtering time of about 750 and 1200 s, respectively, suggesting that more PTB7-Th distribution occurred on the upper surface of the film with 3% DPS. The F^-or S^- signals of the film with 3% DIO were weaker than those without additives and stronger than those with 3% DPS, indicating that less PTB7-Th is distributed at the bottom of the film with 3% DPS. Therefore, it could be inferred that PTB7-Th was mainly distributed in the upper part and $PC_{71}BM$ was mainly concentrated at the bottom of the film with DPS additive, that is, the former decreased with the increase of depth, whereas the latter enhanced with the increase of depth. Combining the results of WCA and TOF-SIMS, DPS could modulate vertical composition distribution of the photoactive layer, which was propitious to ensure the effective carrier dissociation and form an independent carrier transport pathway. Definitely, these observations in vertical composition distribution could partially account for higher FF and J_{SC} obtained in the device-processed 3% DPS additive.

2.4. Charge Generation, Transport, and Recombination. To investigate the mechanism of the additive on exciton generation and dissociation, the photocurrent density of blend films using different processed additives was measured and the corresponding results are shown in Figure 7a,b. These values of the saturated photocurrent density (J_{sat}) at a sufficiently high V_{eff} and the largest exciton generation rate (G_{max}) can be obtained from $G_{maxt} = J_{sat}/qL$,[35] in which q stands for the elementary charge and L represents the thickness of the active layer, and their parameters are listed in Table S2. At V_{eff} = 3 V,

DOI: 10.1021/acsami.8b20466
ACS Appl. Mater. Interfaces XXXX, XXX, XXX–XXX

Table 2. WCA and PTB7-Th Surface Fraction of the Blend Films with Different Additives

	blend film (w/o additives)	blend film (3% DIO)	blend film (3% DPS)	PTB7-Th	$PC_{71}BM$
WCA	94.1°	94.7°	95.0°	98.2°	88.8°
PTB7-Th surface fraction *f*	56.5%	62.9%	66.1%		

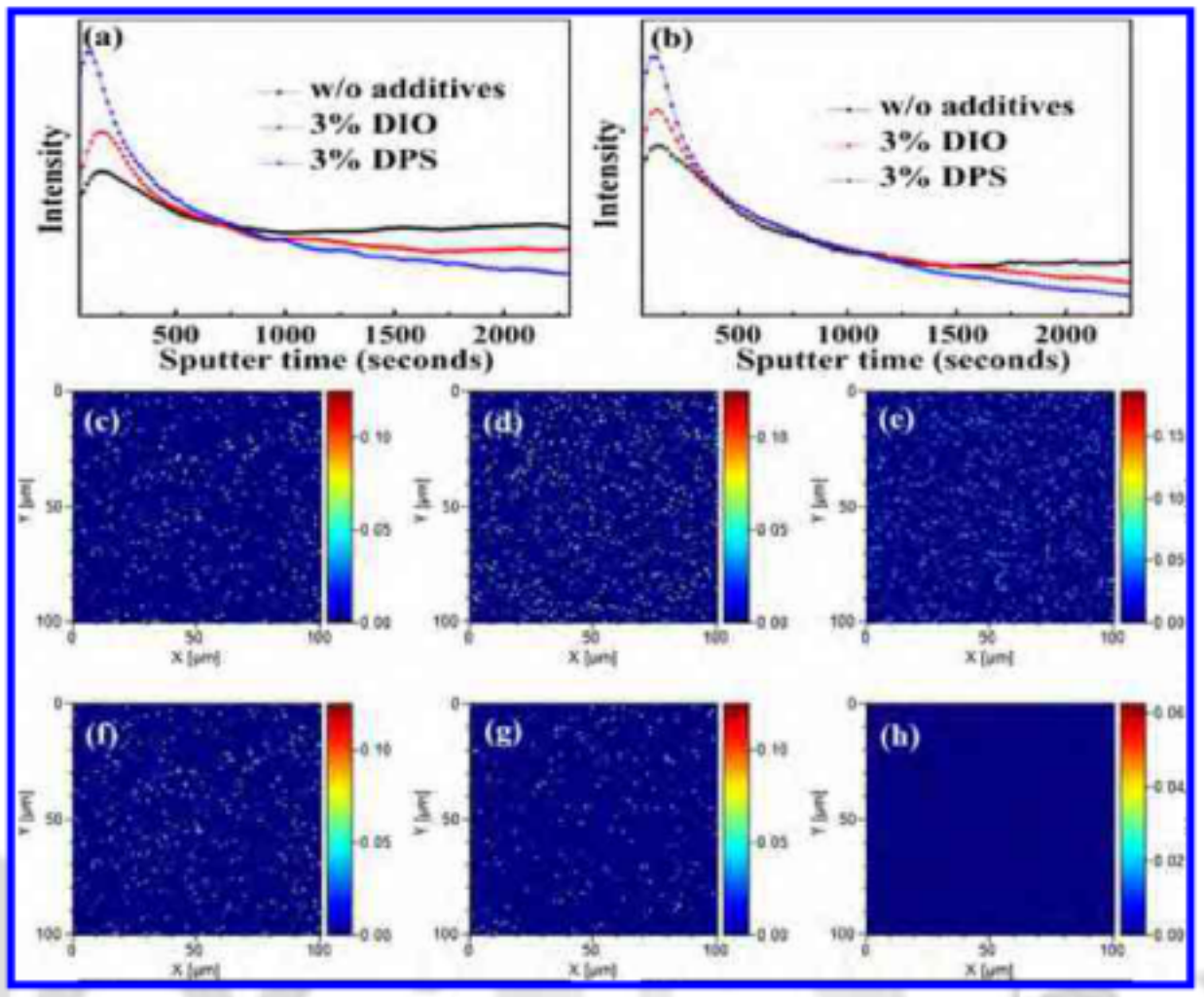

Figure 6. TOF-SIMS data of (a) F^- and (b) S^- in blend films under different conditions. TOF-SIMS images of F^- of the blend film with different additives at 5 s scan (middle row), 2000 s scan (bottom row), (c,f) without additives, (d,g) 3% DIO, and (e,h) 3% DPS.

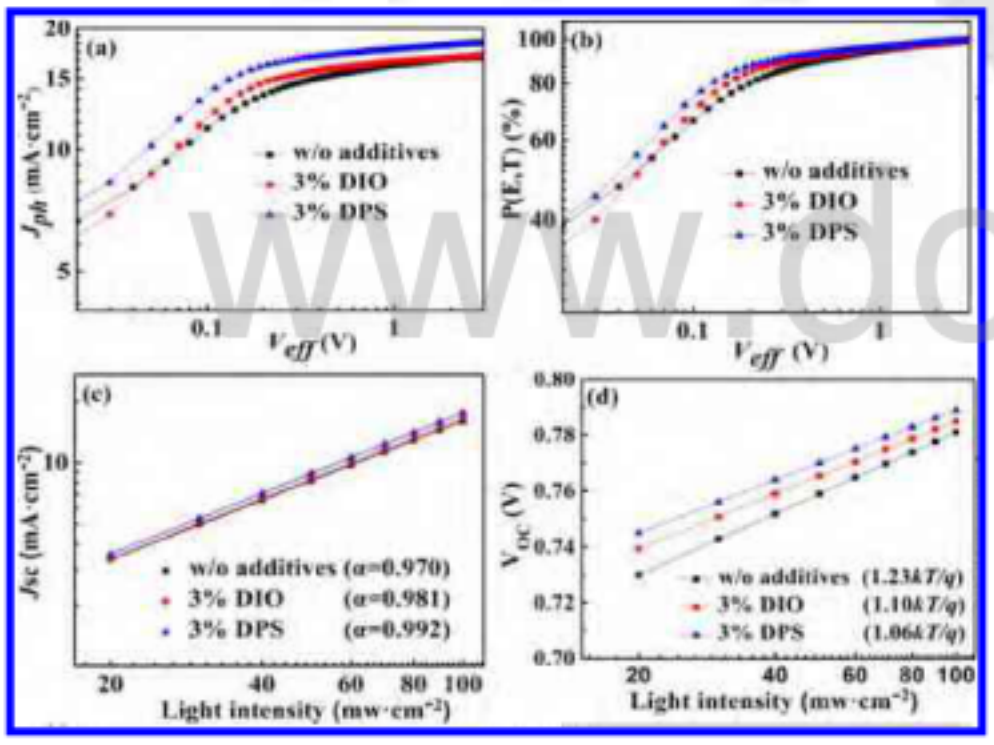

Figure 7. The J_{ph} vs V_{eff}, (b) $P(E,T)$ vs V_{eff}, (c) J_{SC} and (d) V_{OC} vs I curves of the PSCs prepared under different conditions.

the J_{sat} values of the PSCs were 17.0 (without additives), 17.2 (3% DIO), and 18.3 mA·cm^{-2} (3% DPS), corresponding to the G_{max} of 9.64×10^{27}, 9.74×10^{27}, and 1.04×10^{28} m^{-3} s^{-1}, respectively, implying that there were larger exciton generation when the device was fabricated utilizing 3% DPS. Note that the exciton dissociation rate was obtained by the ratio of J_{ph} to J_{sat}. When 3% DIO was added, the exciton dissociation increased from 93.55 to 94.86%, indicating that DIO could slightly improve the exciton dissociated in the interface of the PTB7-Th donor and the $PC_{71}BM$ acceptor. After adding 3% DPS, the maximal exciton dissociation was further enhanced to 95.48%, consistent with the highest J_{SC} and FF obtained from the previous $J-V$ measurement.[36] It was worthy to note that difference in these $P(E,T)$ for the studied devices was small, therefore the enhancement of J_{SC} and FF are probably determined by other reasons.

To investigate the charge recombination mechanism of PSCs, the relationship between J_{SC} or V_{OC} with I of PSCs with different additives was observed. From Figure 7c, the correlation between J_{SC} and light intensity abides by the power law ($J_{SC} \propto I^{\alpha}$), where α is an exponential factor.[37] Note that the value of α is close to 1, indicating that the photogenerated charge carrier under the short-circuit conduction can be effectively extracted and collected by electrodes prior to recombination. In other words, bimolecular recombination is very weak in the photoactive layer.[38−41] The fitted exponential factor (α) values were roughly 0.972, 0.981, and 0.992 for the PSCs without additives, 3% DIO, and 3% DPS, respectively. The decline of bimolecular recombination is probably caused by the morphological rearrangement photoactive layer due to the using of additives, thus boost J_{SC} and FF.[30] The 3% DPS device had an α of 0.992 indicated that the less bimolecular recombination could be demonstrated. The conclusion could be made further efforts to prove by the following formula

$$V_{OC} \propto \frac{nkT}{q} \ln(I)$$

where, k, T, and q are the Boltzmann constant, Kelvin temperature, and the elementary charge, respectively. The slope of the V_{OC} relative to the $\ln(I)$ curve reflects the charge recombination property at open-circuit conditions, when the

DOI: 10.1021/acsami.8b20466
ACS Appl. Mater. Interfaces XXXX, XXX, XXX−XXX

slope is larger than kT/q, trap-assisted recombination becomes more serious.[42,43] From Figure 7d, the slopes of the pristine device with 3% DIO and 3% DPS were 1.23 kT/q, 1.10 kT/q, and 1.06 kT/q. Clearly, the utilization of solvent additives could effectively minimize the reduction of the trap-assisted recombination, and the addition of 3% DPS into the blended film was most pronounced.

To gain deeper insight into the effect of treatments for solvent additives, the vertical charge carrier mobilities were measured from single-carrier devices by fitting the $J-V$ data according to the SCLC method. The detailed $J-V$ curves of hole-only and electron-only devices processed under different conditions are exhibited in Figure 8a,b, and their parameters

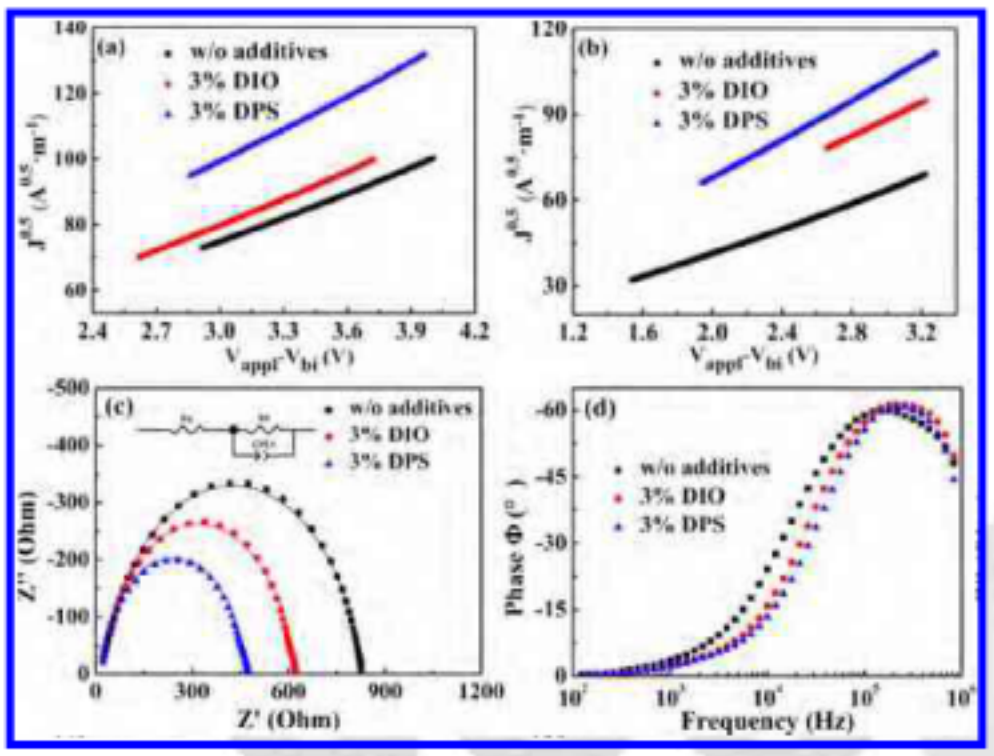

Figure 8. (a) $J-V$ characteristics of hole-only and (b) electron-only, (c) Nyquist plots and (d) Bode phase angle vs frequency plots for PTB7-Th:$PC_{71}BM$-based devices processed without additive, 3% DIO, and 3% DPS, respectively.

are concluded in Table S3. The hole mobility (μ_h) and electron mobility (μ_e) of the blend film without additives were determined to be 2.32×10^{-4} and 1.46×10^{-4} cm^2 V^{-1} s^{-1}, respectively. After adding 3% DIO, μ_h and μ_e values were correspondingly increased to 2.94×10^{-4} and 2.34×10^{-4} cm^2 V^{-1} s^{-1}. Significantly, μ_h and μ_e values continuously enhanced and reached up to 3.93×10^{-4} and 3.82×10^{-4} cm^2 V^{-1} s^{-1}, respectively, when 3% DPS treatment was performed. In addition, the most balanced electron mobility and hole mobility were achieved when the film processed with 3% DPS (Table S3), which were attributed to higher polymer crystallinity and better path of charge carrier transport.[44] It was easy to see that the addition of 3% DPS not only improved the mobility of electrons and holes but also promoted the μ_e/μ_h ratio more balanced, which can explain in part the reason of the greatly improved FF value.

In order to probe carrier dynamics in PSCs processed without additive, 3% DIO, and 3% DPS, IS of these PSC-treated different additives was performed under V_{OC} with an amplitude of 5 mV and frequencies ranging from 100 Hz to 1 MHz in dark conditions. The symbol represents experimental data while the solid line curve denotes fitting data and all Nyquist plots exhibited a semicircle in the complex plan as depicted in Figure 8c. Parameters of the equivalent circuit fitting diagram (Table S4) clearly indicated that this model provided a high quality fitting degree (error rate under 5.7%). In an equivalent circuit, R_S represents resistive losses in the carrier transport layer (PFN and MoO_3) and ITO, correlating with the intersection of the semicircle with Z' axis at high frequencies, so we could observe similar values owing to the identical device architecture. Also, R_1 represents the photoactive layer resistance and decreases with the addition of additives, the best resistance was obtained in the device with 3% DPS. The CPE suggests a nonideal capacitor induced by the inhomogeneity interface. CPE consists of a CPE-T representing the capacitance value and a factor CPE-T relative to the ideal capacitor. Meanwhile, CPE-P was increased from 0.87 to 0.94 with the introduction of 3% DPS, which indicates that the interface capacitance between PTB7-Th and $PC_{71}BM$ is more uniform.[45] As shown in Figure 8d, the characteristic frequency peaks (f_{max}) were located at 146 500 Hz (without additives) and 215 800 Hz (both in 3% DIO and 3% DPS). (Note that the values of f_{max} in the devices with 3% DIO and 3% DPS were identical). The charge transport time constant (τ_{avg}) of PSCs could be derived from the following equation: $f_{max} \propto 1/\tau_{avg}$.[46] Therefore, the PSCs with 3% DIO or 3% DPS had a smaller value of τ_{avg} than of devices without additives. These observations indicated that photogenerated carriers could reach the homologous electrode in PSCs in shorter time and mean a faster carrier transport rate, resulting in the higher efficiency of electronic collection and the greater photocurrent, which is consistent with the best J_{SC} and the highest FF obtained from PSCs with 3% DPS.[47]

To illustrate more deeply and to examine the mechanism of DPS as additives influence the blend, TRTPL spectroscopy was employed to investigate the exciton dissociation kinetics, which can reflect the ultrafast charge transfer process in the nanosecond range. The samples of PTB7-Th:$PC_{71}BM$ blend films prepared under different conditions were excited under 600 nm and probed at 765 nm emission (see Figure 9). The

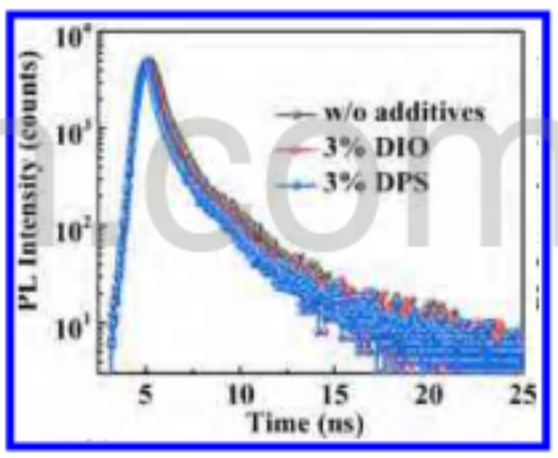

Figure 9. TRTPL spectra of blend films prepared under different conditions.

photoluminescence (PL) decays of the blends exhibit a triple exponential behavior and the fitting results contain two fast sections and one slow section (Table S5). The calculated average lifetime (τ_{ave}) values of without additives, 3% DIO, and 3% DPS are 1.398, 1.236, and 1.169 ns, respectively. The results suggested that after adding additives, the decay life time are decreased, indicating that the excitons are accelerated to splitting to charge.[48] The decay kinetics also indicated that the better bicontinuous interpenetrating network morphology was formed after adding 3% DPS than adding 3% DIO.

3. CONCLUSIONS

In this work, DPS as a novel solvent additive was introduced to enhance the photovoltaic characteristics of PTB7-Th:$PC_{71}BM$-based inverted PSCs. According to the detailed results of TOF-

DOI: 10.1021/acsami.8b20466
ACS Appl. Mater. Interfaces XXXX, XXX, XXX−XXX

SIMS, GIWAXS, WCA, and TEM, we found that the application of DPS is an effective strategy to improve vertical phase segregation and promote crystallinity of the photoactive layer based on PTB7-Th:$PC_{71}BM$, which not only ensured effective exciton dissociation but also the continuous and unhindered path of carrier transport. In addition, it was further confirmed by IS and SCLC that the proposed processing with DPS can not only increase the hole and electron mobility but also optimize the hole-to-electron mobility ratio close to 1.03. These synergistic effects were beneficial to the collection of selective carriers and the reduction of carrier recombination, leading to the best PCE of the PSCs with 3% DPS reach up to 9.7% and an improved FF > 70%. This work suggests that the DPS solvent additive can finely modulate vertical composition distribution and crystallinity of the photoactive layer and improve the photovoltaic performance of the inverted organic photovoltaic devices.

4. EXPERIMENTAL SECTION

PTB7-Th and $PC_{71}BM$ were obtained from Calos and Sigma-Aldrich, respectively. 1,8-Diiodooctane and DPS were purchased from Alfa Aesar and J&K Chemical Ltd., respectively.

These testing conditions and instruments of the thicknesses, $J-V$ curve, EQE, AFM, and TRTPL were all the same as our previous work.[7] TEM images of the thin film were characterized by Tecnai G2 F20 (FEI, USA). GIWAXS was carried out on beamline BL16B1. The IS of devices was performed at an electrochemical workstation (CHI660E, Shanghai Chenhua, China).

■ ASSOCIATED CONTENT

Supporting Information

The Supporting Information is available free of charge on the ACS Publications website at DOI: 10.1021/acsami.8b20466.

Characteristic parameters, $J-V$ characteristics of cells and AFM images with different DPS concentrations (Table S1, Figures S1 and S2, respectively), TOF-SIMS images of S^{2-} of the blend film with different additives at 5 s scan (top row), and 2000 s scan (bottom row), (a,d) without additives, (b,e) 3% DIO, (c,f) 3% DPS (Figure S3), G_{max} and corresponding J_{ph}/J_{sat} values of the PSCs with different additives (Table S2), μ_h, μ_e and μ_h/μ_e of the active layers processed with different additives (Table S3), equivalent circuit model and the impedance spectra fitting parameters (Figure S4 and Table S4, respectively), parameters for TRTPL measurements (PDF)

■ AUTHOR INFORMATION

Corresponding Authors

*E-mail: ljfpyc@163.com (J.L.).
*E-mail: baoxc@qibebt.ac.cn (X.B.).
*E-mail: xiayangjun2015@126.com (Y.X.).

ORCID

Xichang Bao: 0000-0001-7325-7550

Notes

The authors declare no competing financial interest.

■ ACKNOWLEDGMENTS

The authors thank the National Natural Science Foundation of China (no. 51463011), the Natural Science Foundation of Gansu Province (no. 18JR3RA108), Excellent Team of Scientific Research (201705), the Foundation of A Hundred Youth Talents Training. X.B. thanks the Youth Innovation Promotion Association CAS for financial support (2016194).

■ REFERENCES

(1) Zhao, F.; Wang, C.; Zhan, X. Morphology Control in Organic [redacted]. **2018**, *8*, 1703147.

(2) Gao, K.; Deng, W.; Xiao, L.; Hu, Q.; Kan, Y.; Chen, X.; Wang, C.; Huang, F.; Peng, J.; Wu, H.; Peng, X.; Cao, Y.; Russell, T. P.; Liu, F. New Insight of Molecular Interaction, Crystallization and Phase Separation in Higher Performance Small Molecular Solar Cells via [redacted] **2016**, *30*, 639−648.

(3) Liu, D.; Wang, J.; Gu, C.; Li, Y.; Bao, X.; Yang, R. Stirring Up Acceptor Phase and Controlling Morphology via Choosing Appropriate Rigid Aryl Rings as Lever Arms in Symmetry-Breaking Benzodithiophene for High-Performance Fullerene and Fullerene-[redacted] **2018**, *30*, 1705870.

(4) Lee, C.; Lee, H. R.; Choi, J.; Kim, Y.; Nguyen, T. L.; Lee, W.; Gautam, B.; Liu, X.; Zhang, K.; Huang, F.; Oh, J. H.; Woo, H. Y.; Kim, B. J. Efficient and Air-Stable Aqueous-Processed Organic Solar Cells and Transistors: Impact of Water Addition on Processability and Thin-Film Morphologies of Electroactive Materials. *Adv. Energy Mater.* **2018**, *8*, 1802674.

(5) Li, Z.; Xu, X.; Zhang, W.; Meng, X.; Ma, W.; Yartsev, A.; Inganäs, O.; Andersson, M. R.; Janssen, R. A. J.; Wang, E. High Performance All-Polymer Solar Cells by Synergistic Effects of Fine-Tuned Crystallinity and Solvent Annealing. *J. Am. Chem. Soc.* **2016**, *138*, 10935−10944.

(6) Gao, K.; Li, L.; Lai, T.; Xiao, L.; Huang, Y.; Huang, F.; Peng, J.; Cao, Y.; Liu, F.; Russell, T. P.; Janssen, R. A. J.; Peng, X. Deep Absorbing Porphyrin Small Molecule for High-Performance Organic Solar Cells with Very Low Energy Losses. *J. Am. Chem. Soc.* **2015**, *137*, 7282−7285.

(7) Li, J.; Liang, Z.; Wang, Y.; Li, H.; Tong, J.; Bao, X.; Xia, Y. Enhanced Efficiency of Polymer Solar Cells Through Synergistic Optimization of Mobility and Tuning donor Alloys by Adding High-[redacted] **2018**, *6*, 11015−11022.

(8) Xu, X.; Li, Z.; Wang, J.; Lin, B.; Ma, W.; Xia, Y.; Andersson, M. R.; Janssen, R. A. J.; Wang, E. High-Performance all-Polymer Solar Cells Based on Fluorinated Naphthalene diimide Acceptor Polymers with Fine-Tuned Crystallinity and Enhanced Dielectric Constants. *Nano Energy* **2018**, *45*, 368−379.

(9) Bartelt, J. A.; Beiley, Z. M.; Hoke, E. T.; Mateker, W. R.; Douglas, J. D.; Collins, B. A.; Tumbleston, J. R.; Graham, K. R.; Amassian, A.; Ade, H.; Fréchet, J. M. J.; Toney, M. F.; McGehee, M. D. The Importance of Fullerene Percolation in the Mixed Regions of Polymer-Fullerene Bulk Heterojunction Solar Cells. *Adv. Energy Mater.* **2013**, *3*, 364−374.

(10) Ma, W.; Ye, L.; Zhang, S.; Hou, J.; Ade, H. Competition Between Morphological Attributes in the Thermal Annealing and [redacted] **2013**, *1*, 5023−5030.

(11) Ma, W.; Tumbleston, J. R.; Wang, M.; Gann, E.; Huang, F.; Ade, H. Domain Purity, Miscibility, and Molecular Orientation at Donor/Acceptor Interfaces in High Performance Organic Solar Cells: Paths to Further Improvement. *Adv. Energy Mater.* **2013**, *3*, 864−872.

(12) Zhang, M.; Guo, X.; Ma, W.; Zhang, S.; Huo, L.; Ade, H.; Hou, J. An Easy and Effective Method to Modulate Molecular Energy Level of the Polymer Based on Benzodithiophene for the Application in Polymer Solar Cells. *Adv. Mater.* **2014**, *26*, 2089−2095.

(13) Zhang, M.; Guo, X.; Ma, W.; Ade, H.; Hou, J. A Large-Bandgap Conjugated Polymer for Versatile Photovoltaic Applications with High Performance. *Adv. Mater.* **2015**, *27*, 4655−4660.

(14) Chang, L.; Lademann, H. W. A.; Bonekamp, J.-B.; Meerholz, K.; Moulé, A. J. Effect of Trace Solvent on the Morphology of P3HT:PCBM Bulk Heterojunction Solar Cells. *Adv. Funct. Mater.* **2011**, *21*, 1779−1787.

(15) Li, G.; Shrotriya, V.; Huang, J.; Yao, Y.; Moriarty, T.; Emery, K.; Yang, Y. High-Efficiency Solution Processable Polymer Photo-

DOI: 10.1021/acsami.8b20466
ACS Appl. Mater. Interfaces XXXX, XXX, XXX−XXX

voltaic Cells by Self-organization of Polymer Blends. *Nat. Mater.* **2005**, *4*, 864−868.
(16) Park, J. H.; Kim, J. S.; Lee, J. H.; Lee, W. H.; Cho, K. Effect of Annealing Solvent Solubility on the Performance of Poly(3-hexylthiophene)/Methanofullerene Solar Cells. *J. Phys. Chem. C* **2009**, *113*, 17579−17584.
(17) Li, Z.; Xu, X.; Zhang, W.; Meng, X.; Genene, Z.; Ma, W.; Mammo, W.; Yartsev, A.; Andersson, M. R.; Janssen, R. A. J.; Wang, E. 9.0% Power Conversion Efficiency From Ternary all-Polymer Solar [redacted]. **2017**, *10*, 2212−2221.
(18) Deng, W.; Gao, K.; Yan, J.; Liang, Q.; Xie, Y.; He, Z.; Wu, H.; Peng, X.; Cao, Y. Origin of Reduced Open-Circuit Voltage in Highly Efficient Small-Molecule-Based Solar Cells upon Solvent Vapor Annealing. *ACS Appl. Mater. Interfaces* **2018**, *10*, 8141−8147.
(19) Zhu, D.; Bao, X.; Ouyang, D.; Wang, J.; Yuan, X.; Wang, Q.; Zhou, D.; Wen, S.; Yang, R. Single-Junction Fullerene Solar Cells with 10% Efficiency and High Open-Circuit Voltage Approaching 1 V. *Nano Energy* **2017**, *40*, 495−503.
(20) Guo, X.; Cui, C.; Zhang, M.; Huo, L.; Huang, Y.; Hou, J.; Li, Y. High Efficiency Polymer Solar Cells Based on Poly (3-hexylthiophene)/indene-C_{70} Bisadduct with Solvent Additive. *Energy Environ. Sci.* **2012**, *5*, 7943−7949.
(21) Zheng, Y.; Wang, G.; Huang, D.; Kong, J.; Goh, T.; Huang, W.; Yu, J.; Taylor, A. D. Binary Solvent Additives Treatment Boosts the Efficiency of PTB7:PCBM Polymer Solar Cells to Over 9.5%. *Sol. RRL* **2018**, *2*, 170014.
(22) Yao, Y.; Hou, J.; Xu, Z.; Li, G.; Yang, Y. Effects of Solvent Mixtures on the Nanoscale Phase Separation in Polymer Solar Cells. *Adv. Funct. Mater.* **2008**, *18*, 1783−1789.
(23) Yang, K.; Tassone, C. J.; Niskala, J. R.; Yiu, A. T.; Lee, O. P.; Weiss, T. M.; Wang, C.; Fréchet, J. M. J.; Beaujuge, P. M.; Toney, M. F. A Mechanistic Understanding of Processing Additive-Induced Efficiency Enhancement in Bulk Heterojunction Organic Solar Cells. *Adv. Mater.* **2013**, *26*, 300−305.
(24) Xia, Y.; Zhang, H.; Li, J.; Tong, J.; Zhang, P.; Yang, C. Synthesis of Dithieno [2,3-d:2′,3′-d′] benzo[1,2-b:4,5-b′] Dithiophene-alt-isoindigo Conjugated Polymer and Enhancement of Photovoltaic Property with Diphenyl Sulfide Additives. *J. Polym. Res.* **2015**, *22*, 633.
(25) Su, M.-S.; Kuo, C.-Y.; Yuan, M.-C.; Jeng, U.-S.; Su, C.-J.; Wei, K.-H. Improving Device Efficiency of Polymer/Fullerene Bulk Heterojunction Solar Cells Through Enhanced Crystallinity and Reduced Grain Boundaries Induced by Solvent Additives. *Adv. Mater.* **2011**, *23*, 3315−3319.
(26) Wei, S.; Cao, B.; Wang, W.; Moulin, J.-F.; Müller-Buschbaum, P. Effect of Alcohol Treatment on the Performance of PTB7:PC71BM Bulk Heterojunction Solar Cells. *ACS Appl. Mater. Interfaces* **2015**, *7*, 4641−4649.
(27) Guo, S.; Wang, W.; Herzig, E. M.; Naumann, A.; Tainter, G.; Perlich, J.; Müller-Buschbaum, P. Solvent-Morphology-Property Relationship of PTB7:PC71BM Polymer Solar Cells. *ACS Appl. Mater. Interfaces* **2017**, *9*, 3740−3748.
(28) Li, J.; Liang, Z.; Peng, Y.; Lv, J.; Ma, X.; Wang, Y.; Xia, Y. 36% Enhanced Efficiency of Ternary Organic Solar Cells by Doping a NT-Based Polymer as an Electron-Cascade Donor. *Polymers* **2018**, *10*, 703.
(29) Troshin, P. A.; Hoppe, H.; Renz, J.; Egginger, M.; Mayorova, J. Y.; Goryachev, A. E.; Peregudov, A. S.; Lyubovskaya, R. N.; Gobsch, G.; Sariciftci, N. S.; Razumov, V. F. Material Solubility-Photovoltaic Performance Relationship in the Design of Novel Fullerene Derivatives for Bulk Heterojunction Solar Cells. *Adv. Funct. Mater.* **2009**, *19*, 779−788.
(30) Guo, S.; Ning, J.; Körstgens, V.; Yao, Y.; Herzig, E. M.; Roth, S. V.; Müller-Buschbaum, P. The Effect of Fluorination in Manipulating the Nanomorphology in PTB7:PC71BM Bulk Heterojunction Systems. *Adv. Energy Mater.* **2014**, *5*, 1401315.
(31) Yang, X.; Loos, J. Toward High-Performance Polymer Solar Cells: The Importance of Morphology Control. *Macromolecules* **2007**, *40*, 1353−1362.
(32) Liu, F.; Zhao, W.; Tumbleston, J. R.; Wang, C.; Gu, Y.; Wang, D.; Briseno, A. L.; Ade, H.; Russell, T. P. Understanding the Morphology of PTB7:PCBM Blends in Organic Photovoltaics. *Adv. Energy Mater.* **2014**, *4*, 1301377.
(33) Huang, D. M.; Mauger, S. A.; Friedrich, S.; George, S. J.; Dumitriu-LaGrange, D.; Yoon, S.; Moulé, A. J. The Consequences of Interface Mixing on Organic Photovoltaic Device Characteristics. *Adv. Funct. Mater.* **2011**, *21*, 1657−1665.
(34) Cassie, A. B. D.; Baxter, S. Wettability of Porous Surfaces. *Trans. Faraday Soc.* **1944**, *40*, 546−551.
(35) Shrotriya, V.; Yao, Y.; Li, G.; Yang, Y. Effect of Self-Organization in Polymer/Fullerene Bulk Heterojunctions on Solar Cell Performance. *Appl. Phys. Lett.* **2006**, *89*, 063505.
(36) Mihailetchi, V. D.; Koster, L. J. A.; Hummelen, J. C.; Blom, P. W. M. Photocurrent Generation in Polymer-Fullerene Bulk Heterojunctions. *Phys. Rev. Lett.* **2004**, *93*, 216601.
(37) Wang, Y.; Wu, B.; Wu, Z.; Lan, Z.; Li, Y.; Zhang, M.; Zhu, F. Origin of Efficient Inverted Nonfullerene Organic Solar Cells: Enhancement of Charge Extraction and Suppression of Bimolecular Recombination Enabled by Augmented Internal Electric Field. *J. Phys. Chem. Lett.* **2017**, *8*, 5264−5271.
(38) Song, S.; Lee, K. T.; Koh, C. W.; Shin, H.; Gao, M.; Woo, H. Y.; Vak, D.; Kim, J. Y. Hot Slot Die Coating for Additive-free Fabrication of High Performance Roll-to-roll Processed Polymer Solar Cells. *Energy Environ. Sci.* **2018**, *11*, 3248−3255.
(39) Bao, X.; Zhang, Y.; Wang, J.; Zhu, D.; Yang, C.; Li, Y.; Yang, C.; Xu, J.; Yang, R. High Extinction Coefficient Thieno[3,4-b]thiophene-Based Copolymer for Efficient Fullerene-Free Solar Cells with Large Current Density. *Chem. Mater.* **2017**, *29*, 6766−6771.
(40) Chen, W.; Huang, G.; Li, X.; Wang, H.; Li, Y.; Jiang, H.; Zheng, N.; Yang, R. Side-Chain-Promoted Benzodithiophene-based Conjugated Polymers toward Striking Enhancement of Photovoltaic Properties for Polymer Solar Cells. *ACS Appl. Mater. Interfaces* **2018**, *10*, 42747−42755.
(41) Chen, W.; Jiang, H.; Huang, G.; Zhang, J.; Cai, M.; Wan, X.; Yang, R. High-Efficiency Ternary Polymer Solar Cells Based on Intense FRET Energy Transfer Process. *Sol. RRL* **2018**, *2*, 1800101.
(42) Kyaw, A. K. K.; Wang, D. H.; Gupta, V.; Leong, W. L.; Ke, L.; Bazan, G. C.; Heeger, A. J. Intensity Dependence of Current-Voltage Characteristics and Recombination in High-Efficiency Solution-Processed Small-Molecule Solar Cells. *ACS Nano* **2013**, *7*, 4569−4577.
(43) Wan, J.; Xu, X.; Zhang, G.; Li, Y.; Feng, K.; Peng, Q. Highly Efficient Halogen-Free Solvent Processed Small-Molecule Organic Solar Cells Enabled by Material Design and Device Engineering. *Energy Environ. Sci.* **2017**, *10*, 1739−1745.
(44) Peng, K.; Xiao, L.; Kan, Y.; Li, L.; Yan, Y.; Huang, H.; Peng, J.; Cao, Y.; Peng, X. A-π-D-π-A type Small Molecules Using Ethynylene Linkages for Organic Solar Cells with High Open-circuit Voltages. *Chin. J. Chem.* **2016**, *34*, 353−358.
(45) Zheng, Y.; Goh, T.; Fan, P.; Shi, W.; Yu, J.; Taylor, A. D. Toward Efficient Thick Active PTB7 Photovoltaic Layers Using Diphenyl Ether as a Solvent Additive. *ACS Appl. Mater. Interfaces* **2016**, *8*, 15724−15731.
(46) Zhang, Y.; Yuan, S.; Li, Y.; Zhang, W. Enhanced Electron Collection in Inverted Organic Solar Cells using Titanium Oxide/reduced Graphene Oxide Composite Films as Electron Collecting Layers. *Electrochim. Acta* **2014**, *117*, 438−442.
(47) Dunkel, C.; Wark, M.; Oekermann, T.; Ostermann, R.; Smarsly, B. M. Electrodeposition of Zinc Oxide on Transparent Conducting Metal Oxide Nanofibers and its Performance in Dye Sensitized Solar Cells. *Electrochim. Acta* **2013**, *90*, 375−381.
(48) Weu, A.; Hopper, T. R.; Lami, V.; Kreß, J. A.; Bakulin, A. A.; Vaynzof, Y. Field-Assisted Exciton Dissociation in Highly Efficient PffBT4T-2OD: Fullerene Organic Solar Cells. *Chem. Mater.* **2018**, *30*, 2660−2667.

DOI: 10.1021/acsami.8b20466
ACS Appl. Mater. Interfaces XXXX, XXX, XXX−XXX